

Isospin compositions of correlated sources in the Fermi energy domain

R. Ogul,^{1,2} A. S. Botvina,^{3,4} M. Bleicher,^{2,3,4} N. Buyukcizmeci,¹
A. Ergun,¹ H. Imal,¹ Y. Leifels,² and W. Trautmann²

¹*Department of Physics, University of Selçuk, TR-42079 Konya, Turkey*

²*GSI Helmholtzzentrum für Schwerionenforschung GmbH, D-64291 Darmstadt, Germany*

³*Institute for Theoretical Physics, J. W. Goethe University, D-60438 Frankfurt am Main, Germany*

⁴*Helmholtz Research Academy Hesse for FAIR (HFHF), Max-von-Laue-Str. 12, D-60438 Frankfurt am Main, Germany*

(Dated: May 16, 2023)

Isotopic yield distributions of nuclei produced in peripheral collisions of $^{80}\text{Kr}+^{40,48}\text{Ca}$ at 35 MeV/nucleon are studied. Experimental results obtained by the FAZIA Collaboration at the LNS facility in Catania are compared with calculations performed with the statistical multifragmentation model (SMM). The fragments with atomic number $Z = 19 - 24$ observed at forward angles are successfully described with the ensemble method previously established for reactions at higher energy. Using the SMM results, the isotopic compositions of the projectile residues are reconstructed. The results indicate a significant isospin exchange between the projectile and target nuclei, not far from isospin equilibrium, during the initial phase of the reaction. The two groups of light fragments with $Z = 1 - 4$, experimentally distinguished by their velocities relative to coincident heavy projectile fragments, are found to originate from different sources. The isotopic composition of the slower group is consistent with emission from a low-density neck, enriched in neutrons, and satisfactorily reproduced with SMM calculations for a corresponding neck source of small mass.

PACS numbers: 25.70.Mn, 25.70.Pq, 21.65.Ef

I. INTRODUCTION

There is continuing high interest in investigating the nuclear fragment production in heavy-ion collisions of intermediate energies [1, 2]. It is a typical many-body process in which the nuclear interaction can manifest its ingredients and lead to important states of matter. The fragment production mechanisms, the properties of nuclear matter at both high and low densities, new reaction products, e.g., exotic isotopes, and their correlations can be addressed [2, 3]. The theoretical explanations of these phenomena include various methods involving dynamical and statistical approaches. In such complicated many-body processes, phenomena governed by interactions of both, high and low energy coexist. Their description may go beyond the capabilities of one specific model. It is, therefore, important to determine correctly the regions of applicability for each model and to explore alternatives to reach a comprehensive picture.

The technical achievements of the FAZIA Collaboration have widened the possibilities for reaction studies at intermediate energies [4–6]. By extending the limits of mass and charge resolution of telescope-type detection units, arrays with large solid-angle coverage have become available for new experiments exploring the role of isospin in heavy-ion collisions [7, 8]. Isospin transfer between the reaction partners reflects the action of the symmetry parts of the nuclear forces [2, 9, 10]. Studying their effects requires isotopic identification of the reaction products. It has been known for a long time that product distributions respond to the isotopic properties of the primary source, whose composition, however, may be concealed by secondary-decay effects [11, 12].

In a first experiment addressing isospin transport at

intermediate energies, the FAZIA Collaboration studied the fragment production in ^{80}Kr collisions with ^{48}Ca and ^{40}Ca targets at 35 MeV/nucleon beam energy [4]. Four detector cubes equipped with the FAZIA technology were placed at forward angles. The chosen inverse kinematics had the effect of focusing projectile fragments into forward directions efficiently covered by the FAZIA modules.

The analysis of the data was aimed at extracting the density dependence of the symmetry-energy term in the nuclear equation of state. For this purpose, the antisymmetrized molecular dynamics (AMD) transport model and the statistical decay code GEMINI were used and “a weak indication in favor of a stiff symmetry energy” was reported. At densities below saturation, the stiff solution corresponds to lower values for the symmetry energy. However, comparison with the experimental data shows that the isotopic composition of the observed fragments is not much influenced by the symmetry-energy term and depends mainly on the statistical processes at the later reaction stages. For this reason, we believe it is instructive to perform an alternative analysis of the experimental results in order to clarify the role of the statistical breakup and decay in the formation of the final products.

The present work attempts an interpretation of the same data aiming at the isospin transfer during the contact time between the reaction partners. The isotopic composition of the primary reaction products will be determined from the observed products by modeling the deexcitation of the former with the statistical multifragmentation model (SMM, Ref. [13]). The SMM is capable of following various reaction scenarios from compound evaporation through fission and multifragmentation up

to vaporization according to the statistical weights given to these paths in the model description. It thus represents a rather universal model which was previously successfully applied for the description of the fragment production in peripheral and central heavy ion collisions at relativistic energies [14–17] and in the Fermi energy domain (Refs. [18–21] and references given therein).

To describe the projectile fragments, the calculations start from an ensemble of excited sources whose properties, mainly the isotopic composition, is varied until an optimum description of the measured isotopic distributions for projectile fragments with atomic numbers $Z = 19 - 24$ is achieved. The peripheral character of the data has encouraged us to attempt an extrapolation of the method found useful for reactions at higher energies [14, 16] to the present case. It differs from an earlier theoretical study of peripheral $^{112}\text{Sn} + ^{124}\text{Sn}$ and $^{124}\text{Sn} + ^{112}\text{Sn}$ reactions in which sources with fixed mass and charge were used as initial configurations for SMM calculations [22].

Normalized relative yields of light fragments from the same experiment are also presented in the FAZIA publication [4]. They were recorded in coincidence with a heavy fragments of $Z \geq 12$ ($Z > 18$ in the case of $^{80}\text{Kr} + ^{40}\text{Ca}$) and sorted into two groups depending on whether their longitudinal velocities are larger or smaller than those of the coincident heavy fragment. Considering that fragments with $Z = 3$ or 4 included in the faster group are not typical evaporation products, their origin is not immediately obvious. The slower group extends up to $Z = 11$ and thus covers the Z interval of intermediate mass fragments abundantly produced in multifragmentation processes. Their neutron content $\langle N \rangle / Z$ as a function of Z exhibits the odd-even staggering known from other reactions, revealing a neutron richness exceeding that of the projectile sources. To explain these fragments we assume the formation of a highly excited statistical source forming a neck between the target and the projectile [23]. With SMM calculations based on this scenario, the observed isotopic composition is very satisfactorily reproduced.

II. FRAGMENT PRODUCTION IN THE STATISTICAL APPROACH

Presently there are two main statistical conceptions intending to describe the physics of fragment production as a decay of excited finite nuclei. The most popular one is that of the compound nucleus [24] which decays with the sequential emission of light particles. There are several mathematical formalisms according to this conception which can be used for practical calculations. For example, GEMINI [25, 26] uses the Hauser-Feshbach method, while SMM uses the Weisskopf method for the low-energy emission. As was shown in the theoretical and experimental studies, the compound nucleus conception works very well from low excitation energy of nuclei up

to values around 2 to 3 MeV/nucleon [13, 27].

Another conception was mainly developed in the 1980s (see, e.g., reviews [13, 28] and references therein), and we may call it the freeze-out-volume conception. It was motivated by intensive experimental studies of the multifragmentation process leading to the production of many intermediate mass fragments from the decay of a highly excited nuclear source.

According to the freeze-out-volume conception, the compound nucleus has no time to be formed, since the highly excited nucleus rapidly expands (on a time scale of approximately 100 fm/c), and the system breaks-up (re-forms itself) into fragments during this expansion. The last moment at which the fragments can still be considered as interacting and being under formation is the statistical freeze-out time. Subsequently the fragments propagate in the mutual Coulomb fields and undergo secondary deexcitation as usual for low-excited nuclei. SMM includes this conception and thus provides an opportunity to describe multifragmentation data. Since we are dealing with finite nuclear systems, a weak point of the freeze-out-volume conception up to now was that the upper limit of the excitation energy was not determined. In this case, the very idea of applying statistical laws in the rapidly expanding matter is not convincing from a theoretical view.

A method for solving this problem was suggested recently: By analyzing the fragment production in central nucleus-nucleus collisions at beam energies of more than 50–100 MeV/nucleon, it was established that the maximum excitation energy of such statistical sources can not reach more than 8–10 MeV/nucleon [29, 30]. This compares well with the previous maximum excitation energy of sources found in peripheral and central collisions. It is consistent with the binding energy of finite nuclei, providing the natural physical limit for the application of the statistical theory. In our case of nucleus-nucleus collisions at the Fermi energy, such energies correspond to the maximum energy reached in the center of mass of the colliding nuclei.

According to the statistical hypothesis, initial dynamical interactions between the colliding nuclei lead to a redistribution of the available energy among many degrees of freedom. The nuclear system evolves towards equilibrium. In a general consideration, the process may be subdivided into two stages: (1) a dynamical stage leading to the formation of an equilibrated nuclear system, and (2) the statistical disassembly of the system into individual primary fragments, followed by their deexcitation and the formation of the final product distribution observed in experiments.

Dynamical models indicate that individual reactions at intermediate energies are not evolving as equilibrium processes [31]. However, because of the complexity of the dynamical processes, the intermediate reaction states populate a phase space that can be described with very few parameters, and whose disassembly according to statistical laws leads to the observed asymptotic state of the re-

action [32]. By applying the SMM, a scenario is adopted that places the equilibrium state at an early stage of the reaction, before the partitioning of the excited system occurs. The parameters describing the equilibrium state thus contain information on global properties of the initial reaction stages forming it. The present study aims at identifying the isospin transport during this early part of the collision.

Sequences of statistical decay processes are expected to proceed towards the valley of stability at which binding energies reach their maximum. More precisely, the expected asymptotic destination is represented by the evaporation attractor line (EAL), whose location is mainly determined by the competition between proton and neutron evaporation [33]. Often, and also in the present case, the decay sequences are not long enough, so that the EAL is approached but not fully reached.

The emission of fragments is treated in the SMM by expanding the excited sources to the statistical freeze-out volume. This is assumed to be caused by thermal pressure or as a decompression process after an initial dynamical collective compression. However, a similar low-density freeze-out state of nuclear matter may also be created through the stochastic knock-out of nucleons produced by initial nucleon-nucleon collisions. The freeze-out density is expected to be around $(0.1\text{--}0.3)\rho_0$, where $\rho_0 \approx 0.16 \text{ fm}^{-3}$ is the normal nuclear density. The value of $0.3\rho_0$ has been adopted for the projectile sources as in previous analyses [14–16].

Peripheral reactions at the present intermediate energies are additionally characterized by a low-density third source of nucleons and light fragments located at intermediate velocities [23, 34–39]. It may contain products of nucleon-nucleon collisions removed from the main residues as well as remnants of necklike structures joining projectile and target residues before they separate. Interpreted as a continuation of the multifragmentation mechanism towards intermediate impact parameters, the processes at intermediate velocity seem suitable for a statistical description with the SMM, an approach rarely attempted up to now [40]. The neutron content of these sources is of specific interest because of the expected neutron drift toward regions of lower density caused by the density dependence of the symmetry energy [41, 42].

III. METHOD

In Ref. [4], the FAZIA Collaboration reports the relative isotope distributions for elements with $Z = 19 - 24$, individually normalized for each atomic number Z . They were measured with four FAZIA detector blocks placed at forward angles between $\theta_{\text{lab}} = 2.4^\circ$ and 17.4° , covering approximately 14% of the solid angle up to $\theta_{\text{lab}} = 17.4^\circ$ (see Ref. [43] for a layout of the experiment). In the present analysis, we assume that the fragment distributions recorded within the covered solid angle are representative for projectile fragmentation in the studied reac-

tions. The same is assumed for the coincident light fragments with atomic numbers $Z \leq 4$ and $Z \leq 11$ recorded with the same setup for two velocity regimes.

The velocities of the $Z = 19 - 24$ fragments are shown to be only slightly lower than the initial velocity of the ^{80}Kr projectiles. This, together with their masses of more than half of the projectile mass, identifies them as resulting from peripheral processes. One may thus expect that their masses are correlated and their excitation energies inversely correlated with the impact parameter. Such correlations are reminiscent of the participant-spectator scenario established for reactions at higher energies. It is, therefore, further assumed that the equilibrated intermediate state can be described with an ensemble of sources with properties similar to those determined in the analysis of projectile fragmentation at energies up to 1 GeV/nucleon [14–17].

The ensemble consists of a distribution of sources extending from systems of low excitation and masses near the projectile mass to highly excited systems of small mass expected to be formed in central collisions, and, in this form, is universally applicable (Fig. 1). The form of its peripheral branch with excitation energies up to $\approx 4 \text{ MeV/nucleon}$ compares well with AMD predictions for comparable reactions [44] and the general energy-mass correlation is consistent with transport model predictions up to much higher energies [45]. The fragments of interest and their distributions are selected from the output configurations obtained from the eventwise performed calculations for the full ensemble.

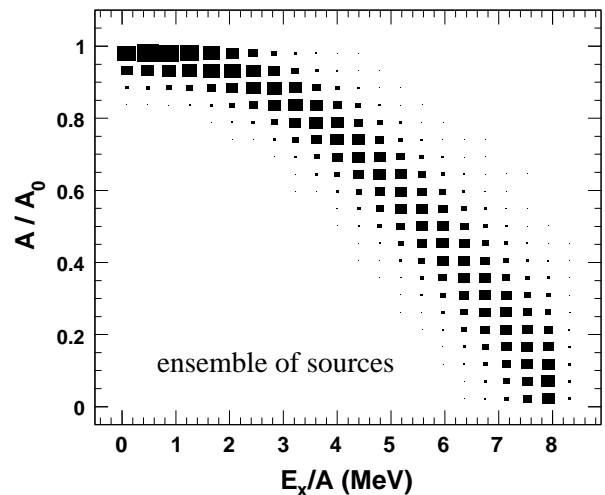


FIG. 1: Ensemble of hot thermal sources represented in a scatter plot of reduced mass number A/A_0 versus excitation energy E_x/A , as used in the SMM calculations. The frequency of the individual sources is proportional to the area of the squares (reprinted with permission from Ref. [16]; copyright © 2011 by the American Physical Society).

Altogether, seven parameters are required to define the ensemble of excited sources. In the analyses performed

with the ALADIN data for projectile fragmentation at energies up to 1 GeV/nucleon, the experimental data permitted a determination of these parameters with very little ambiguity as shown in Refs. [14, 16]. This is not possible here, and the general form of the ensemble was, therefore, adopted from the earlier work. The maximum mass $A_0 = 80$ and atomic number $Z_0 = 36$ are those of the projectile, assuming that pickup processes are rare at the present energies. Also the maximum excitation energy $E_x/A = 8$ MeV was chosen as in previous studies and as supported by recent work [29, 30]. It is not crucial, however, because the event selection requiring a fragment with $Z \geq 12$ and $Z \geq 19$ for the two reactions implies that the excited projectile residues compose at least about half of the original projectile. The excitation energies of such sources with $A/A_0 \geq 0.5$ are limited to values near or below 4 MeV/nucleon (Fig. 1). As in previous studies (see, e.g., Refs. [18–22]), angular momentum is not considered as an independent property of the source because its effects are small and, regarding the isotopic fragment distributions, indistinguishable from the much larger effects of the excitation energy.

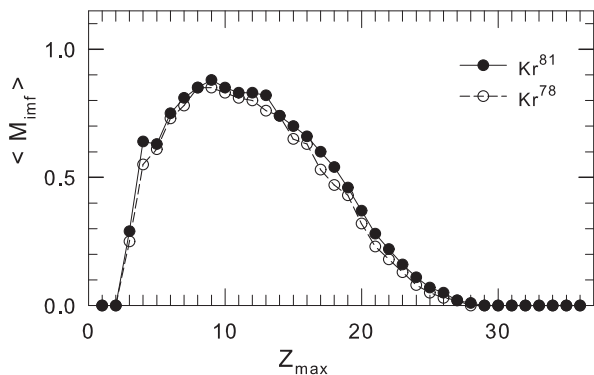


FIG. 2: Mean multiplicity $\langle M_{\text{imf}} \rangle$ of fragments of intermediate mass with $Z \geq 3$ in coincidence with the fragment with the largest atomic number Z_{max} found in an event as a function of Z_{max} , as obtained with the SMM for the fragmentation of the projectile in $^{81}\text{Kr} + ^{48}\text{Ca}$ (solid circles) and $^{78}\text{Kr} + ^{48}\text{Ca}$ (open circles).

The experimental data [4] were collected without a particular impact-parameter selection, even though peripheral collisions are favored by the detection at forward angles. Correspondingly, the whole ensemble of excited projectile residues is taken into account in the analysis, and the element range of interest is selected from the calculated set of final products. For exploring the isospin transfer during the initial reaction stage, the mean composition $\langle N/Z \rangle$ was varied by varying the maximum mass A_0 without changing Z_0 . It is assumed that the associated small change in E_x/A vs A , caused by the construction of the ensemble, is negligible for the narrow interval of fragments with $Z = 19 - 24$.

The isotope yields depend also on the properties of the

primary hot nuclei in the statistical freeze-out. In this respect the most important ingredient is the symmetry term of their liquid-drop description and its coefficient γ . The symmetry term governs the widths of isobaric or isotopic fragment distributions [46, 47]. The standard value used in SMM applications is $\gamma \approx 25$ MeV [13, 48]. Similar but also lower values have been determined from statistical interpretations of reaction data at lower [49, 50] and higher energy. The isoscaling analysis of fragmentation reactions with Sn targets and light-ion beams of up to 15 GeV incident energy resulted in $\gamma = 22.5$ MeV [47]. From the isoscaling analyses performed for $^{12}\text{C} + ^{197}\text{Au}$ reactions at 300 and 600 MeV/nucleon [51] and for the fragmentation of $^{107,124}\text{Sn}$ and ^{124}La projectiles on Sn targets at 600 MeV/nucleon [16] values of $\gamma = 15$ MeV and lower were deduced. The lowest values, however, were found for the most violent collisions and for fragments with $Z \leq 10$. A similar scenario is not expected in the present case for the production of fragments with $Z = 19 - 24$ in peripheral collisions at 35 MeV/nucleon. As will be shown below, γ can be determined rather precisely from the widths of the measured isotope distributions.

In a first step, the calculations were used to confirm that the chosen procedure permits satisfactory reproductions of the experimental isotope distributions and to obtain global properties of the reaction. As an example, the multiplicity of fragments of intermediate mass produced in coincidence with a largest fragment with atomic number Z_{max} is shown in Fig. 2. The chosen threshold is $Z \geq 3$ and the upper limit is either Z_{max} or $36 - Z_{\text{max}}$, whichever is smaller. Fragments in this interval are not typical for evaporation but, according to the calculations, are produced with mean multiplicities close to 1 for Z_{max} around 10. In the interval covered by the experiment, $Z_{\text{max}} \geq 12$ and $Z_{\text{max}} \geq 19$ for the two reactions, the mean multiplicity of associated fragments decreases from about 0.8 to very small values at the upper end of the range of Z_{max} . The multiplicity widths are probably large and the production of intermediate mass fragments cannot be expected to be negligible.

In a second step, the sensitivity of the mean mass number of the produced projectile fragments to the isotopic compositions of the chosen ensembles was explored. The compositions reveal the results of isospin transport phenomena during the initial phases of the collision, the main goal of the present study. The capabilities of the SMM [13] to describe the statistical disassembly of the intermediate system and the subsequent modes of deexcitation permits a view back on to these early reaction stages through backtracing from the detected fragmentation patterns. In a third step, the origin of the coincident light fragments was investigated by comparing their mean neutron-over-proton ratios to the results obtained for ^{107}Sn and ^{124}Sn fragmentations in experiment S254 conducted at the GSI laboratory [16].

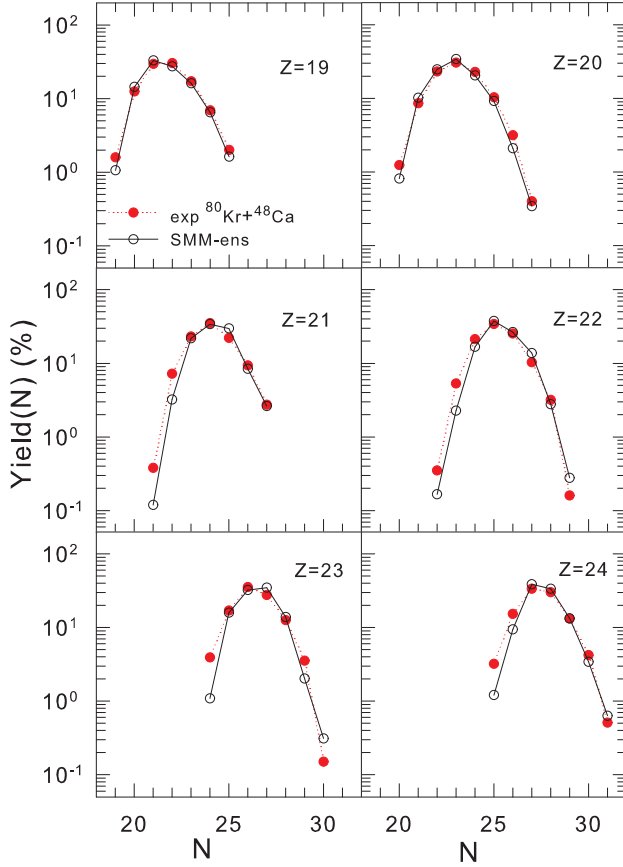


FIG. 3: Comparison of the predicted isotopic distributions of fragments with $Z = 19 - 24$ with the experimental data measured in the $^{80}\text{Kr} + ^{48}\text{Ca}$ reaction. The solid red circles represent the experimental data from Ref. [4] and open circles the results of the SMM-ensemble calculations for the same reaction.

IV. COMPARISON WITH THE EXPERIMENT

The results obtained in the first step are presented in Figs. 3 to 6. The isotopic distributions of nuclei in the interval of atomic numbers $Z = 19 - 24$ for collisions of $^{80}\text{Kr} + ^{48}\text{Ca}$ and $^{80}\text{Kr} + ^{40}\text{Ca}$ are shown in Figs. 3 and 4, respectively. The normalized isotopic yield distributions measured in the FAZIA experiments [4] are represented by solid circles. For the SMM calculations represented by the open circles, it was assumed that the projectile ^{80}Kr picks up an extra neutron from the ^{48}Ca target and loses two neutrons in interactions with the ^{40}Ca target, or that an equivalent exchange of nucleons takes place. With the corresponding parameters for the maximum mass of the projectile $A_0 = 81$ and 78 and with $Z_0 = 36$, average compositions $\langle N/Z \rangle = 1.25$ and 1.17 were thus assumed for the two cases, respectively.

Other parameters describing the ensemble of sources were fixed as in Ref. [16]. Specifically, for the coefficient γ of the symmetry term, values of $\gamma = 18$ MeV for $Z = 19 - 20$, $\gamma = 19$ MeV for $Z = 21 - 22$, and

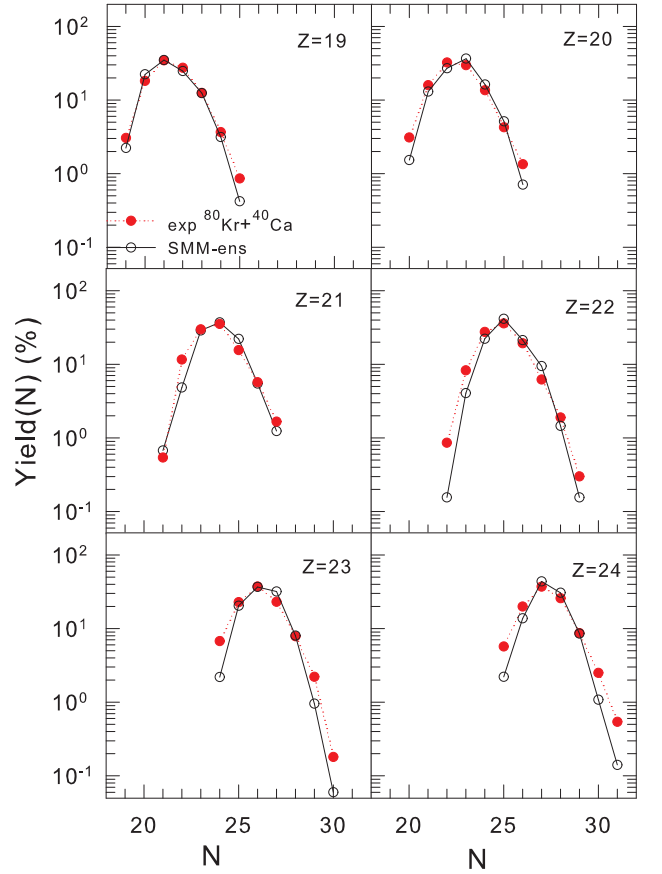


FIG. 4: Comparison of the predicted isotopic distributions of fragments with $Z = 19 - 24$ with the experimental data measured in the $^{80}\text{Kr} + ^{40}\text{Ca}$ reaction. The solid red circles represent the experimental data from Ref. [4] and open circles the results of the SMM-ensemble calculations for the same reaction.

$\gamma = 20$ MeV for $Z = 23 - 24$ were found to provide the results closest to the experimental data for $^{80}\text{Kr} + ^{48}\text{Ca}$ and values larger by 1 MeV for $^{80}\text{Kr} + ^{40}\text{Ca}$. The figures demonstrate that the chosen procedure permits a rather satisfactory reproduction of the experimental isotope distributions for the products of mid-peripheral collisions with atomic number $Z = 19 - 24$.

The same ensemble nuclei were also used to calculate isotopic distributions of light fragments with $Z = 1 - 4$. The distinction made in the experiment between particles emitted into forward or backward directions with respect to the coincident heavier fragment cannot be applied in the model calculations but the coincidence with a heavier fragment was required. In the case of $^{80}\text{Kr} + ^{48}\text{Ca}$, only events containing a fragment with atomic number Z between 12 and 36 and, for $^{80}\text{Kr} + ^{40}\text{Ca}$, only events containing a fragment with Z between 19 and 36 were selected.

Figures 5 and 6 show the calculated relative isotopic yields of light nuclei with $Z = 1 - 4$ in comparison with the experimental yields for fragments with longitudinal

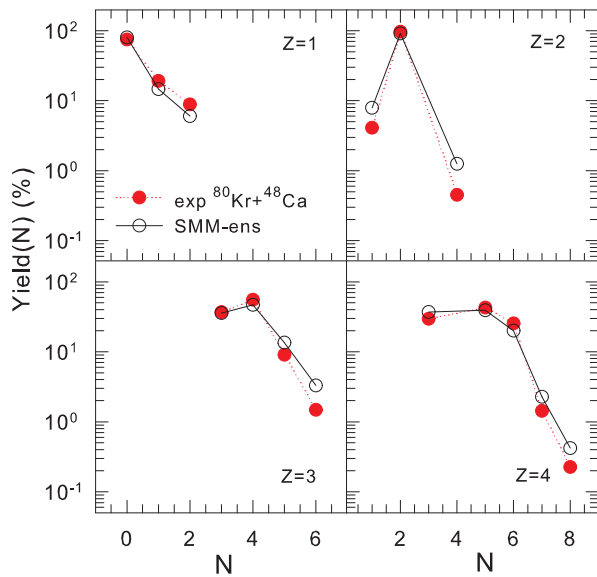


FIG. 5: Isotopic yield distributions for light nuclei with atomic number $Z = 1 - 4$, emitted forward with respect to the coincident projectile residue in the $^{80}\text{Kr} + ^{48}\text{Ca}$ reaction. Red solid circles represent the experimental data of Ref. [4], and open circles represent the results of the SMM-ensemble calculations.

velocities larger than those of the coincident heavier fragment. Protons and α particles obviously dominate the distributions of hydrogen and helium isotopes. In both reactions, ^7Li is the strongest lithium isotope while ^9Be is the strongest beryllium isotope only in the $^{80}\text{Kr} + ^{48}\text{Ca}$ reaction and is equally abundant as ^7Be in the $^{80}\text{Kr} + ^{40}\text{Ca}$ reaction. Overall, the observed differences between the two reactions appear to be small. The results of the SMM-ensemble calculations represent the experimental data rather well. On a logarithmic scale, deviations are essentially only visible in the cases of helium and lithium isotopes. Some of the predictions for weak isotopes slightly overestimate the experimental yields. These yields play a minor role for the mean neutron-over-proton ratios shown for the $Z = 1 - 4$ products in Fig. 7. The agreement is best for $Z = 2$, obviously so because of the dominance of ^4He , and overall very satisfactory.

V. SYMMETRY COEFFICIENT γ

Within the SMM, the statistical disintegration of highly excited nuclei includes the expansion of the nuclear system into a freeze-out volume within which the primary hot fragments are formed and the chemical equilibrium (i.e., the detailed-balance interaction) between them is established. The properties of these hot fragments can be different from those of cold stable nuclei. In particular, their symmetry-term coefficients γ can be lower than the standard value of 25 MeV that is taken in the liquid-drop Bethe-Weizsäcker formula describing

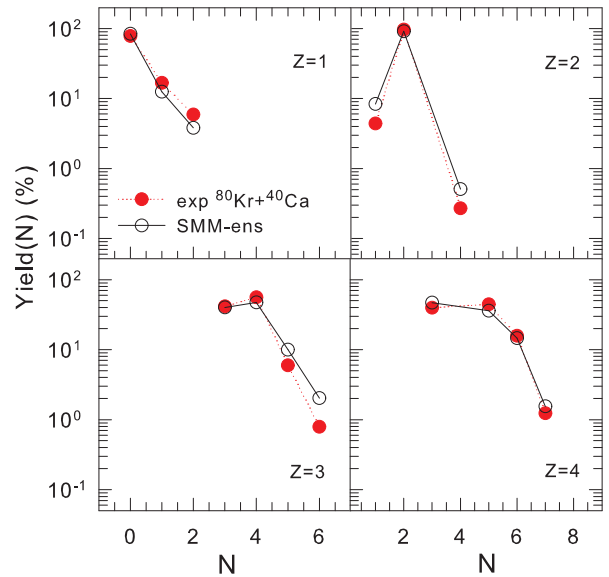


FIG. 6: Isotopic yield distributions for light nuclei with atomic number $Z = 1 - 4$, emitted forward with respect to the coincident projectile residue in the $^{80}\text{Kr} + ^{40}\text{Ca}$ reaction. Red solid circles represent the experimental data of Ref. [4], and open circles represent the results of the SMM-ensemble calculations.

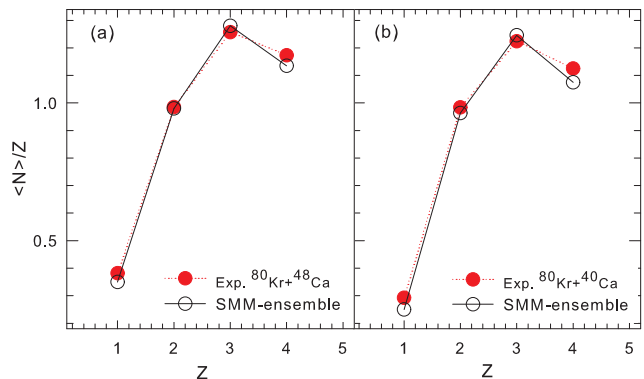


FIG. 7: Experimental and theoretical results for the $\langle N \rangle / Z$ ratios of light fragments, emitted forward with respect to the coincident projectile residue, obtained in the $^{80}\text{Kr} + ^{48}\text{Ca}$ and $^{80}\text{Kr} + ^{40}\text{Ca}$ reactions as presented in Figs. 5 and 6. Red solid circles represent the experimental data and open circles represent the results of the SMM-ensemble calculations.

masses of normal nuclei (see, e.g., Refs. [13, 47–51]). The reason is that the fragments are interacting until freeze-out, they can be slightly expanded, and their surface parts can be extended. Subsequently, the standard value of the symmetry-term coefficient is restored during the secondary deexcitation of the hot fragments [48].

The coefficient γ controls the widths of the calculated isotope distributions [46, 47]. This is illustrated in Fig. 8, which shows the examples of isotopic yields for $Z = 19$ calculated for $A_0 = 78$ and values of $\gamma = 8$,

19, and 25 MeV in comparison with the experimental data obtained in $^{80}\text{Kr} + ^{40}\text{Ca}$. It is evident that the widths change significantly with γ and that the value $\gamma = 19$ MeV chosen for this case leads to the good reproduction of the data seen in Fig. 4. It is also evident that the Gaussian fits included in the figure permit a quantitative analysis of the distribution widths. The dependence of the Gaussian standard deviations on γ is illustrated in the top panel of Fig. 9. It confirms that $\gamma = 19$ MeV for $Z = 19$ is rather precisely, with an uncertainty of around ± 1 MeV, determined by the measured data. The dependence of the mean neutron number $\langle N \rangle$ on γ , equally evident in Fig. 8, is given in the bottom panel of Fig. 9.

The widths of some of the isotope distributions appear to be slightly underpredicted by the calculations (Figs. 3 and 4). An adjustment of γ in these cases requires the simultaneous modification of the mean $\langle N \rangle / Z$ that is to be expected. The variations of the widths and mean neutron numbers with γ , shown for $Z = 19$ in Fig. 9, are rather universal and very similar for the studied elements with $Z = 19 - 24$. Further individual optimizations of specific parameters may lead to a slightly different ensemble of excited sources representing the intermediate reaction systems.

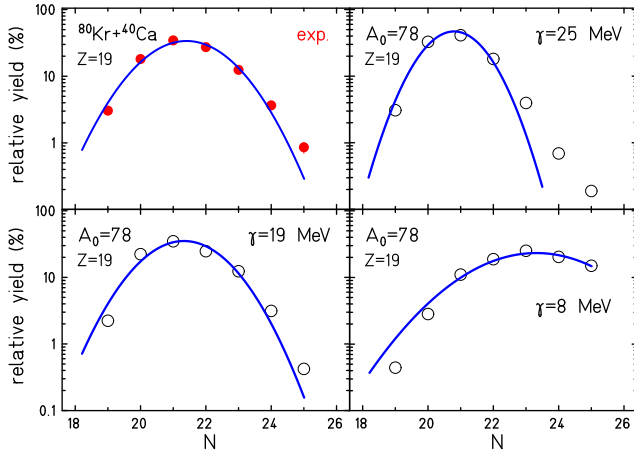


FIG. 8: Relative yield distributions for $Z = 19$ and the results of Gaussian fits (blue lines) as measured in $^{80}\text{Kr} + ^{40}\text{Ca}$ (top left panel, red solid circles) and as calculated with $A_0 = 78$ and the indicated values of the symmetry-term coefficient γ (open circles). The errors of the experimental data are mostly smaller than the symbol size.

The values $\gamma = 18 - 21$ MeV applied in the present calculations had already been found useful for describing projectile fragments of similar magnitude from $^{112,124}\text{Sn} + ^{112,124}\text{Sn}$ collisions at 1 GeV/nucleon [17]. They are also close to the Z dependent symmetry-term coefficients used in the microcanonical multifragmentation model [52] and in the AMD model [53]. The surface term included in the AMD leads to $\gamma = 20.4$ MeV and 21.2 MeV for $Z = 19$ and 24, respectively, assuming $A = 2Z$. The AMD coefficients were determined by fitting the ground state binding energies for $A \leq 40$ nuclei

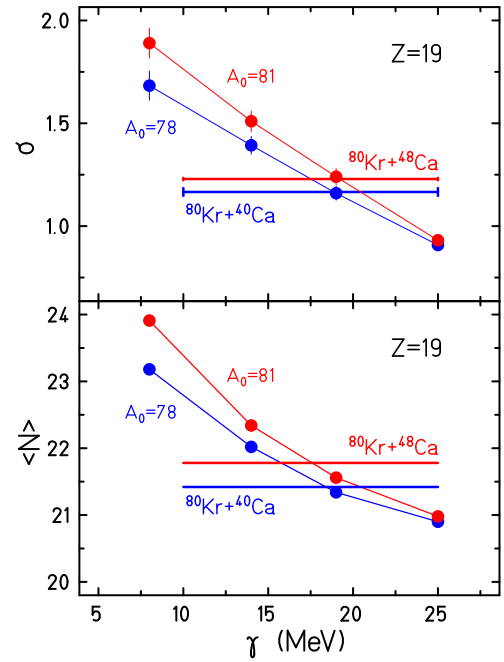


FIG. 9: The standard deviation σ of the Gaussian functions fitted to the measured and calculated isotope distributions in units of the neutron number (top) and the mean neutron number $\langle N \rangle$ (bottom) as a function of the symmetry-term coefficient γ used in calculations for $Z = 19$ with $A_0 = 78$ and 81 (filled circles). The horizontal lines indicate the results deduced from the experimental data including their uncertainties which, for the case of $\langle N \rangle$, are smaller than the line widths.

calculated with the AMD model. In the present case, the symmetry term is part of the description of the produced nuclear fragments with excitation energies up to about 4 MeV/nucleon. The difference of the coefficients is, however, marginal.

VI. INITIAL COMPOSITIONS

The initial compositions defined by choosing $A_0 = 78$ and 81 indicate a considerable amount of isotopic equilibration between projectile and target during the early stages of the two reactions, more than 60% of full isospin equilibrium. For a more quantitative analysis, the N/Z compositions of the ensembles of excited sources were investigated by varying the A_0 parameter from 75 to 83 while keeping $Z_0 = 36$ fixed. It covers the interval of initial compositions $\langle N/Z \rangle_{\text{ini}} = A_0/36 - 1$ from 1.083 to 1.306. The subscript "ini" is used here and in the following to indicate the initial isotopic composition at the beginning of the statistical decay modeled with the SMM.

The calculated fragment yields were normalized, as in the experimental report [4], and the sum of the quadratic deviations from the measured values in units of the ex-

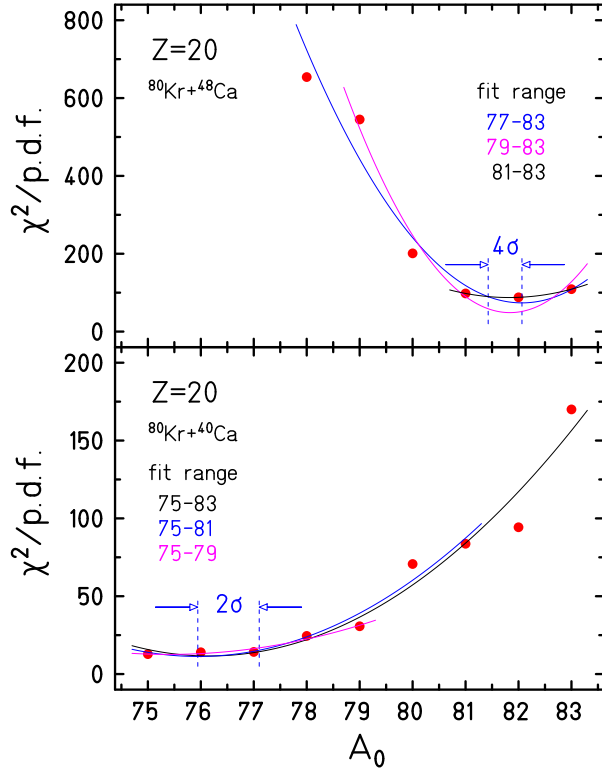


FIG. 10: Mean quadratic deviations (χ^2 per degree of freedom) of the relative isotopic yields for $Z = 20$ projectile fragments with mass numbers $A = 40 - 46$ as a function of the A_0 parameter used for varying the initial composition $\langle N/Z \rangle_{\text{ini}}$ of the ensemble of sources for the two reactions $^{80}\text{Kr} + ^{48}\text{Ca}$ (top) and $^{80}\text{Kr} + ^{40}\text{Ca}$ (bottom). The lines are the results of parabolic fits performed for three different intervals of A_0 as indicated in each panel. The uncertainty intervals obtained for the fits extending over seven data points (blue lines) corresponding to 4σ in the upper and 2σ in the lower panel, are shown for illustration.

perimental errors was determined for each of the sets obtained with a given A_0 . The so obtained χ^2 distribution was divided by the number of isotopes considered for a given Z , reduced by one because of the normalization. The result for the example of $Z = 20$ fragments is shown in Fig. 10 for the two studied reactions. The displayed distributions of χ^2 per degree of freedom exhibit the expected parabolic behavior. Their absolute values are rather large because the quoted experimental errors are very small [4], considerably smaller for the data obtained with the ^{48}Ca target than for the data obtained with the ^{40}Ca target.

The minima of the parabolic fits (Fig. 10) determine the optimum composition of the ensemble of sources as approximately $N/Z_{\text{ini}} = 1.28$, obtained with $A_0 = 82$, for the fragmentation on the ^{48}Ca target and $N/Z_{\text{ini}} = 1.11$ obtained with $A_0 = 76$ for the ^{40}Ca case. They are similar to the original assumptions but indicate an even larger degree of equilibration. By analyzing the fits for the intervals extending over seven data points (represented by

TABLE I: Summary of the results obtained for the initial configurations $\langle N/Z \rangle_{\text{ini}}$ by comparing the calculated mean neutron numbers $\langle N \rangle$ with the experimental value (fourth column) or by searching for the minimum of the χ^2 distribution obtained with the experimental errors (last column). The prediction of the evaporation attractor line [33] is shown in the third column.

^{48}Ca		$\langle N/Z \rangle_{\text{ini}}$		$\langle N/Z \rangle_{\text{ini}}$
Z	$\langle N \rangle_{\text{exp}}$	N/Z_{EAL}	from $\langle N \rangle_{\text{exp}}$	from χ^2
19	21.78 ± 0.01	1.116	1.278 ± 0.003	1.300 ± 0.005
20	23.11 ± 0.01	1.118	1.292 ± 0.002	1.280 ± 0.004
21	24.10 ± 0.01	1.121	1.209 ± 0.002	1.215 ± 0.007
22	25.23 ± 0.01	1.123	1.206 ± 0.002	1.198 ± 0.006
23	26.39 ± 0.01	1.125	1.210 ± 0.002	1.207 ± 0.007
24	27.49 ± 0.01	1.128	1.220 ± 0.002	1.244 ± 0.009
weighted mean			1.232 ± 0.001	1.254 ± 0.002

^{40}Ca		$\langle N/Z \rangle_{\text{ini}}$		$\langle N/Z \rangle_{\text{ini}}$
Z	$\langle N \rangle_{\text{exp}}$	N/Z_{EAL}	from $\langle N \rangle_{\text{exp}}$	from χ^2
19	21.42 ± 0.02	1.116	1.207 ± 0.011	1.169 ± 0.017
20	22.53 ± 0.02	1.118	1.098 ± 0.008	1.110 ± 0.016
21	23.77 ± 0.02	1.121	1.067 ± 0.010	1.126 ± 0.013
22	24.92 ± 0.02	1.123	1.060 ± 0.011	1.115 ± 0.014
23	26.10 ± 0.02	1.125	1.072 ± 0.006	1.113 ± 0.016
24	27.21 ± 0.02	1.128	1.103 ± 0.007	1.113 ± 0.023
weighted mean			1.101 ± 0.003	1.124 ± 0.006

the blue lines), $A_0 = 77 - 83$ for ^{48}Ca and $A_0 = 75 - 81$ for ^{40}Ca , the compositions $N/Z_{\text{ini}} = 1.280 \pm 0.004$ and $N/Z_{\text{ini}} = 1.110 \pm 0.016$ are obtained for the two cases, respectively. The corresponding 4σ and 2σ widths are indicated in the figure.

The results obtained for the six elements are given in the last column of Table I. The reconstructed intermediate configurations of the excited projectile systems are fairly neutron rich for $^{80}\text{Kr} + ^{48}\text{Ca}$ and fairly neutron poor for $^{80}\text{Kr} + ^{40}\text{Ca}$. The weighted mean values are 1.254 and 1.124, respectively, with a difference much larger than naively expected from the fairly similar experimental isotope distributions (Figs. 3 and 4; see also Fig. 6 in Ref. [4]). It is obvious that the individual errors obtained for each element are not representative for the element-to-element variations. For further use, we therefore chose to give equal weight to each of the elements for determining the mean values and to adopt the mean squared deviations from the mean divided by $\sqrt{5}$ as their uncertainties. With this choice, the compositions obtained with the χ^2 method are $\langle N/Z \rangle_{\text{ini}} = 1.241 \pm 0.017$ and 1.124 ± 0.009 for the two reactions. Their difference amounts to $82 \pm 14\%$ of the difference between the fully equilibrated compositions.

In addition to the χ^2 analysis employing the experimental errors, the measured and calculated mean mass numbers for each of the six elements were used to confirm the obtained results. The example for the same $Z = 20$ case and for the two reactions is shown in Fig. 11. The figure, first of all, documents the strong attenuation of the initial N/Z ratios caused by the breakup and deexcitation of the excited sources as modeled with the SMM. Significantly different compositions of the hot sources (red symbols) are required for obtaining the small differences of the experimental mean fragment masses. The comparison of the experimental $\langle N \rangle/Z$ with the values for cold fragments obtained with the SMM (blue symbols), identifies $A_0 = 82$ and $A_0 = 76$ as A_0 parameters coming closest to reproducing the experimental mean fragment masses for $Z = 20$. The corresponding compositions $\langle N \rangle/Z_{\text{ini}} = 1.278$ and 1.111 are nearly the same as those of the χ^2 analysis (Table I).

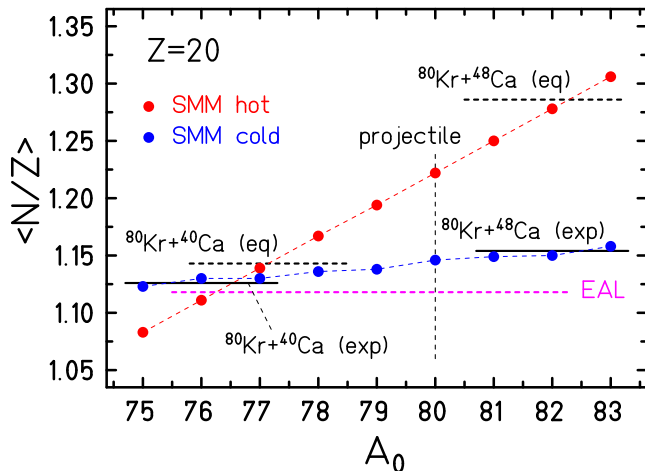


FIG. 11: Mean isotopic compositions $\langle N/Z \rangle_{\text{ini}}$ of the initial systems (hot, red symbols) and the $\langle N \rangle/Z$ of the final $Z = 20$ isotope distributions obtained with the SMM (cold, blue symbols) as a function of the maximum mass A_0 of the chosen ensembles. The calculated results are compared with the experimental mean neutron-over-proton ratios (labeled “exp”, full black lines) for both reactions and the EAL prediction (dashed purple line) for $Z = 20$ fragments. The compositions corresponding to the isotopically equilibrated projectile and target systems (labeled “eq”, dashed black lines) are shown in addition.

To find the optimum composition for each element, linear fits to the three calculated mean $\langle N \rangle/Z$ closest to the experimental value were used and the final result determined with a linear interpolation. The results obtained in this way for the six elements are also shown in Table I (fourth column). The displayed uncertainties are very small, reflecting again the precision of the experimental mean neutron numbers. For obtaining more realistic uncertainties, the method used in the χ^2 analysis was adopted. Equal weights were given to the results for each of the elements, and the uncertainty of the mean composition determined by dividing the mean squared devi-

ations of the six individual values by $\sqrt{5}$. The obtained compositions $\langle N/Z \rangle_{\text{ini}} = 1.236 \pm 0.016$ and 1.101 ± 0.022 for the two reactions are, within their errors, compatible with the results obtained with the χ^2 method. The difference amounts to $94 \pm 17\%$ of the difference between the equilibrated systems. The weighted average of the results obtained with the two methods corresponds to $87 \pm 11\%$ of the difference between the equilibrated systems.

To arrive at a lower limit for the degree of equilibration following from the present study, a possible effect of the symmetry-term coefficient γ has to be included. On average, we find that $\Delta\gamma = +1$ MeV causes $\langle N \rangle$ to decrease by approximately 0.10 and vice versa (cf. Fig. 9). Following Fig. 11, it translates into an uncertainty $\Delta\langle N \rangle/Z \approx 0.005$ and $\Delta\langle N/Z \rangle_{\text{ini}} \approx 0.031$, equivalent to 22% of the difference between the equilibrated systems. This uncertainty is larger but is only effective if changes of γ are different in the two reactions by a certain amount, for example additionally increased by 1 MeV only in the case of $^{80}\text{Kr} + ^{40}\text{Ca}$. A global change of γ will only change the vertical position of the line describing the calculated final compositions but not its slope determining the separation of the two experimental values on this line. Adopting this possibility as cause for an additional uncertainty leads to a lower bound of 87% -11% -22% = 54% for the degree of equilibration reached in the two reactions.

According to the analysis presented here, rapid N/Z equilibration during the initial reaction stage seems necessary for reaching the observed final isotopic distributions. This conclusion depends crucially on the rate with which the mean $\langle N \rangle/Z$ of fragments (blue symbols in Fig. 11) increases with $\langle N/Z \rangle_{\text{ini}}$, a result of the treatment of secondary decay within the SMM. We also note that, for both reactions, the initial compositions are less neutron rich than the equilibrated systems. As we will argue below, it may be caused by the drift of neutrons into a neck region of low density which is no longer involved in the disintegration of the projectile residues.

As evident from Fig. 11, the breakup and deexcitation of the hot sources proceeds very differently in the two cases. There is very little variation of the isotopic composition in the $^{80}\text{Kr} + ^{40}\text{Ca}$ case. The hot and cold SMM values of $\langle N/Z \rangle$ and the experimental value are all very close to the equilibrium composition and not far from the value of the evaporation attractor line [33]. In the case of $^{80}\text{Kr} + ^{48}\text{Ca}$, the neutron richness of the excited system disappears to a large extent but, also here, the evaporation attractor line is not fully reached. The valley of stability attracts the decay chains but they are not long enough to end on the evaporation attractor line. Apparently, since the multifragmentation mechanism favors the production of neutron rich fragments, the deposited energy is primarily used for the disintegration of the system into smaller fragments instead of neutron evaporation.

VII. NECK EMISSIONS

In Ref. [4], the group of coincident light fragments with longitudinal velocities smaller than those of the coincident heavy fragments is interpreted as either being emitted in backward direction from the excited projectile residue or as representing emissions from the intermediate velocity source, the latter containing products of nucleon-nucleon collisions and from the decay of the neck forming as the main residues separate [23]. In the data analysis, the additional condition was required that the velocities had to be larger than the center-of-mass velocity.

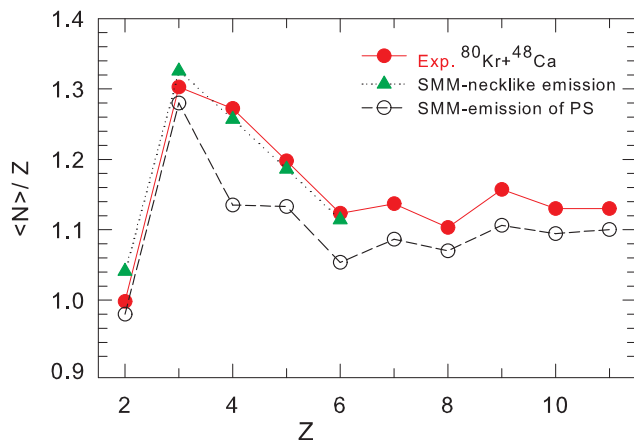


FIG. 12: Experimental $\langle N \rangle / Z$ values of neck fragments as a function of their charge number $Z = 2 - 11$ for the $^{80}\text{Kr} + ^{48}\text{Ca}$ reaction, in Ref. [4] defined as fragments emitted backward with respect to the projectile residue (solid red circles), and results of SMM calculations simulating the decay of a neck-type source with $A = 19$ and properties given in the text for the interval $Z = 2 - 6$ (solid green triangles) in comparison with the results for $Z = 2 - 11$ of the projectile source (PS) with $A = 81$ and $Z = 36$, selected with the requirement of a coincident fragment with $Z \geq 12$ (open circles).

The $\langle N \rangle / Z$ ratios for fragments with $Z = 2 - 11$ are among the data reported for this group of fragments and, for the $^{80}\text{Kr} + ^{48}\text{Ca}$ reaction, shown in Fig. 12. As the authors note, the observed pattern as a function of Z is well known from other studies and, as an example, the work of Barlini *et al.* [54] is cited in [4]. The same characteristic odd-even staggering has also been observed in projectile fragmentation at higher energies. The systematics presented in Ref. [55] for projectiles from nickel to uranium and energies of 600 MeV/nucleon and 1 GeV/nucleon shows that the pattern is invariant and that only its location on the N/Z scale depends on the projectile, apparently linearly correlated with the N/Z ratio of the projectile. In Ref. [55], a correction for the missing yield of unstable ^8Be was applied to the values for $Z = 4$ by including an estimate for it obtained from a smooth interpolation over the identified yields of $^{7,9-11}\text{Be}$. This correction has a negligible effect for the case of ^{107}Sn but

lowers the $\langle N \rangle / Z$ of beryllium for ^{124}Sn fragmentations from 1.24 to 1.18 which makes the systematic odd-even staggering more clearly visible for the neutron rich case.

For the interpretation of the fragmentation reactions at relativistic energies, it may be assumed that the excited sources inherit the neutron-over-proton ratio of the original projectiles. It is motivated by the reduced nucleon wave lengths, the dominance of nucleon-nucleon dynamics during the initial reaction stages, and was shown to be successful in applications as, e.g., the SMM analysis of the $^{107,124}\text{Sn}$ and ^{124}La fragmentations at 600 MeV/nucleon [16]. It implies that the systematics obtained for light fragments may be used for calibrating the isotopic compositions of the excited sources.

In the following, we will assume that the observed correlation between sources and fragments holds for the present type of reactions as well. The statistical decay of excited sources should only depend on their properties and not on how they were formed. With the measured $\langle N \rangle / Z$ values for products with $3 \leq Z \leq 9$ from the ^{107}Sn and ^{124}Sn fragmentations displayed in Fig. 3 of Ref. [55], a source reconstruction is attempted, not only for the so-called backward emitted group of light fragments (Fig. 12) but also for the forward emitted fragments whose $\langle N \rangle / Z$ ratios for $Z = 1 - 4$ are shown in Fig. 8 of [4] and reproduced in the present Fig. 7. In the latter case, the overlap in atomic number with the $^{107,124}\text{Sn}$ fragmentations is restricted to $Z = 3$ and 4. The corresponding $\langle N \rangle / Z$ ratios for backward emitted fragments from $^{80}\text{Kr} + ^{40}\text{Ca}$ are obtained by adding the backward-forward differences shown in Fig. 11 of [4].

The results for the two elements $Z = 3$ and 4 are listed in Table II. They are obtained by assuming that the values measured for the ^{107}Sn and ^{124}Sn fragmentations, given in the first two lines of Table III, are representative for source compositions $\langle N/Z \rangle = 1.16$ and 1.48, respectively, and that a linear interpolation between (or extrapolation from) these values is appropriate. The value $\langle N/Z \rangle = 1.16$ for the case of ^{107}Sn refers to the actual radioactive beams used in the experiment which, besides the desired ^{107}Sn , contained contributions of neighboring isotopes whose intensities had been determined [16, 56].

As a main conclusion, we observe that the sources responsible for the so-called backward-emitted fragments in both reactions are significantly more neutron rich than the sources responsible for the forward-emitted fragments. Simply on the basis of the obtained neutron-over-proton ratios, it can thus be excluded that both groups of fragments have the same origin. In the case of $^{80}\text{Kr} + ^{48}\text{Ca}$, the average composition $\langle N/Z \rangle = 1.51$ of the backward-emitted fragments is still significantly larger than the value 1.31 expected for a mixed source consisting of equal numbers of nucleons from the projectile and from the target. The same holds for $^{80}\text{Kr} + ^{40}\text{Ca}$. Also here the average composition $\langle N/Z \rangle = 1.37$ largely exceeds the value 1.11 of an equally mixed source. The values obtained for the forward-emitted particles, on the other hand, are in approximate agreement with the re-

TABLE II: Reconstruction of the composition of the emitting sources obtained with the measured $\langle N \rangle/Z$ ratios of $Z = 3, 4$ fragments presented in Figs. 8, 11, and 12(a) of Ref. [4] (third and fifth columns) and based on the inclusive $\langle N \rangle/Z$ ratios measured for $^{107,124}\text{Sn}$ fragmentations in experiment S254 (first two lines of Table III). For beryllium, the uncorrected $\langle N \rangle/Z$ ratios have been extracted from the ALADIN data base. The source compositions are obtained by linear interpolations and extrapolations (fourth and sixth columns). Their errors represent the effects of the displayed experimental errors reported in Ref. [4].

group	target	$Z = 3$ (Expt.)	Source	$Z = 4$ (Expt.)	Source
		$\langle N \rangle/Z$	$\langle N/Z \rangle$	$\langle N \rangle/Z$	$\langle N/Z \rangle$
forward	^{48}Ca	1.255 ± 0.003	1.29 ± 0.02	1.180 ± 0.006	1.38 ± 0.01
backward	^{48}Ca	1.300 ± 0.002	1.49 ± 0.01	1.273 ± 0.003	1.53 ± 0.01
forward	^{40}Ca	1.224 ± 0.009	1.15 ± 0.04	1.109 ± 0.020	1.27 ± 0.03
backward	^{40}Ca	1.274 ± 0.016	1.38 ± 0.07	1.170 ± 0.032	1.37 ± 0.05

sults for the fragments with $Z = 19 - 24$ shown in Table I. It permits the conclusion that the latter two groups of fragments result from the breakup of the same excited intermediate sources.

The errors displayed in Table II are those of the experimental data reported in Ref. [4] and their effect on the reconstructed source compositions. These errors are very small. To obtain an estimate of a potential systematic uncertainty associated with the method, $\langle N \rangle/Z$ ratios for $Z = 5 - 9$ from the fragmentation of $^{124,136}\text{Xe}$ projectiles on Pb targets are used which had been measured at the GSI Fragment Separator FRS [57]. Reconstructing the source compositions on the basis of the $^{107,124}\text{Sn}$ results for the same $Z = 5 - 9$ fragments (Table III) leads to values consistently higher by $\Delta N/Z = 0.09$ than the N/Z ratios of the $^{124,136}\text{Xe}$ projectiles, corresponding to almost five additional neutrons. The difference $\Delta N/Z = 0.23$ between the results for the two Xe projectiles, however, is very close to the actual difference $\Delta N/Z = 0.22$ of their N/Z ratios. Relative differences are preserved but the absolute values, according to this test, are shifted by $\Delta N/Z \approx 0.1$. For the following discussion, the source compositions listed in the tables will be reduced by $\Delta N/Z = 0.05$ and an error of equal magnitude will be assigned to them. It is equivalent to giving equal weights to the Sn and Xe fragmentations in their role for the intended reconstruction of source compositions.

This uncertainty does not affect the resulting implications. The so-called backward emitted particles are unlikely to originate from the same source as the forward emitted particles and light fragments. This was also concluded by the FAZIA Collaboration and reported in their paper [4]. The neutron richness of the backward sources is enhanced even in comparison to those of the equally mixed sources by corrected values $\Delta \langle N/Z \rangle \approx 0.15$ in the case of $^{80}\text{Kr} + ^{48}\text{Ca}$ and ≈ 0.21 in the case of $^{80}\text{Kr} + ^{40}\text{Ca}$. If this is caused by neutrons drifting into these sources their densities will have to be low, a property expected for the neck region located between

TABLE III: Reconstruction of the neutron-over-proton ratios of the emitting sources (fifth column) obtained with the $\langle N \rangle/Z$ ratios of $Z = 3 - 9$ fragments presented in Fig. 12 of Ref. [4] (second column) and based on the inclusive $\langle N \rangle/Z$ ratios measured for $^{107,124}\text{Sn}$ fragmentations in experiment S254 as reported in Ref. [55] (third and fourth columns). For beryllium, the uncorrected $\langle N \rangle/Z$ ratios have been extracted from the ALADIN data base. The errors of the sources represent the effects of the displayed experimental errors reported in Ref. [4].

Z	Expt.	^{107}Sn	^{124}Sn	Source
3	1.300 ± 0.002	1.227	1.297	1.494 ± 0.009
4	1.273 ± 0.003	1.038	1.243	1.527 ± 0.005
5	1.196 ± 0.001	1.134	1.200	1.461 ± 0.005
6	1.122 ± 0.001	1.037	1.138	1.429 ± 0.003
7	1.137 ± 0.001	1.103	1.153	1.378 ± 0.006
8	1.103 ± 0.001	1.048	1.120	1.404 ± 0.004
9	1.158 ± 0.002	1.132	1.190	1.303 ± 0.011

the separating projectile and target residues [23]. Even its mass may be estimated by taking into account that the compositions of the projectile sources were, on average, lower than those of the equilibrated systems by $\Delta \langle N/Z \rangle \approx 0.035$, a change achieved by the drift of two neutrons out of a system with together 56 protons. The same two neutrons will raise the neutron-over-proton ratio by ≈ 0.18 , the average enhancement observed for the two reactions, in a smaller system with only about one fifth the number of protons. The mass of the neck region, according to this estimate, should thus be of the order of $(\langle N/Z \rangle + 1) \times 56 \times 0.035/0.18$, i.e., about 25 nucleons.

The obtained source properties are very consistent. Going more into detail, one observes that the values for the sources of $Z = 4$ fragments are systematically larger than those for the sources of $Z = 3$ fragments. On the

other hand, the calibration for $Z = 3$ amplifies small differences and thus may be associated with a larger uncertainty (cf. Table II). Elements with odd Z generally respond less strongly to the source composition, according to the data published in Ref. [55] which extend up to $Z = 9$. It is thus possible to extend the calibration to heavier fragments of the so-called backward emitted group in $^{80}\text{Kr} + ^{48}\text{Ca}$ whose composition is presented in the FAZIA report [4].

The results, again obtained with linear interpolations and extrapolations, are given in Table III. The obtained compositions are all neutron rich, starting with values $\langle N \rangle / Z \approx 1.5$ for $Z = 3$ and 4 and slowly decreasing with Z to values 1.4 and 1.3 for the $Z = 8$ and 9 fragments, respectively. A dependence on Z of this kind is not unexpected considering the so-called hierarchy effect according to which the lightest fragments are expected from the regions of lowest density in between the projectile and target rapidities [23, 34, 58]. The scatter of the individual results may be used as indication of their systematic uncertainty.

It will finally be shown that SMM calculations of the deexcitation of a neck-type source with properties corresponding to these results will lead to light fragment yields with $\langle N \rangle / Z$ ratios in good agreement with the FAZIA measurement for the $^{80}\text{Kr} + ^{48}\text{Ca}$ reaction [4]. Following a series of test calculations with varying parameters for the masses and excitation energies of the source as well as for its $\langle N/Z \rangle$ composition, the following scenario was assumed: a fixed mass $A = 19$ and atomic number $Z = 8$ of the source, corresponding to $N/Z = 1.375$, an excitation energy of 5 MeV/nucleon, a reduced breakup density $\rho = \rho_0/6$, and a reduced symmetry-term coefficient $\gamma = 14$ MeV were considered as appropriate for the small masses of the produced fragments. Similar parameters were found useful in previous SMM studies of multifragmentation reactions [13, 18, 19]. For example, in central $^{197}\text{Au} + ^{197}\text{Au}$ collisions at the same beam energy of 35 MeV per nucleon, a statistical source with the same density and excitation energy per nucleon was extracted [18].

The obtained $\langle N \rangle / Z$ ratios for neck fragments with $Z \leq 6$ are shown in Fig. 12, and a very satisfactory agreement with the experimental results is observed. For comparison, the results for the projectile source (PS) with $A = 81$ and $Z = 36$ ($N/Z = 1.25$) is shown as well. They are obtained from the same calculation as the results shown in Figs. 5 and 7 and seen there to agree well with the experimental results for the forward emitted coincident fragments. The characteristic odd-even staggering is apparent in both calculations as nuclear structure effects are taken into account in the SMM for the ground-state masses which are restored at the end of the secondary deexcitation.

The significant difference in $\langle N \rangle / Z$ with respect to the experimental values for the class of slower fragments, documented for $Z = 3, 4$ in Table II, is found to extend to larger Z . The modest reduction of the difference toward

$Z = 11$ is not unexpected. Neck fragments are predominantly small as already mentioned in the discussion related to Table III. It thus appears that the definition of two groups by the FAZIA Collaboration represented a very useful choice, giving evidence for the existence of different sources of coincident light fragments. The sorting according to the sign of the relative velocity is clearly not sufficient for precisely distinguishing particles and fragments according to their various origins, as discussed in detail in the paper [4].

VIII. DISCUSSION

The indicated isotopic exchange between projectile and target seems somewhat unexpected on the basis of the measured isotope distributions exhibiting rather small differences. The latter are the consequence of the attraction of the valley of stability which causes the initial neutron richness of the excited sources in $^{80}\text{Kr} + ^{48}\text{Ca}$ to quickly disappear (Fig. 11). Large contributions of the target to measured isotopic ratios of light fragments have already been observed in the earlier experiment of the FAZIA Collaboration [54]. At that time, a three-element telescope placed at $\theta_{\text{lab}} = 5.4^\circ$ was used to measure inclusive fragment production in the $^{84}\text{Kr} + ^{112,124}\text{Sn}$ reactions at 35 MeV/nucleon. The observed $\langle N \rangle / Z$ values of light fragments depend significantly on the target. For lithium and beryllium fragments, values of ≈ 1.3 are reported with differences of ≈ 0.03 for the two target cases.

Applying the same method of source reconstruction as for the present reaction leads to rather neutron rich sources with $\langle N/Z \rangle_{\text{ini}} = 1.63$ and 1.46 for the reactions with ^{124}Sn and ^{112}Sn targets, respectively. These values are higher than in the present reactions (Tables II or III) as expected for the more neutron rich projectile. They are also higher than the $\langle N/Z \rangle_{\text{ini}} = 1.42$ and 1.28 of the equilibrated $^{84}\text{Kr} + ^{124,112}\text{Sn}$ systems and their difference 0.17 exceeds even slightly the difference 0.14 of the latter. Following the interpretation offered in the previous section, one would, therefore, conclude that these light fragments are primarily emitted from low-density regions of the reaction volume whose neutron content has been enhanced. According to the analysis of the slightly heavier Xe+Sn reaction by Lukasik *et al.* [36], the very light fragments have their origin predominantly in the midrapidity regime.

Isotopic equilibrium is not unusual in the Fermi energy domain. It was, for example, observed by Johnston *et al.* for inclusive reactions of Ar and Ca beams of mass $A = 40$ on Fe and Ni targets of mass $A = 58$ and incident energies 33 MeV/nucleon [59]. As shown in that work, when the energy is increased to 45 MeV/nucleon full equilibrium is no longer achieved. Partial equilibrium was observed also in the cross bombardment of ^{112}Sn and ^{124}Sn beams and targets at the slightly higher beam energy of 50 MeV/nucleon by Tsang *et al.* [60]. Partial isospin equilibrium of $\approx 53\%$ was reported by Keksis *et*

al. for $^{40,48}\text{Ca}$ on $^{112,124}\text{Sn}$ reactions at the slightly lower energy 32 MeV/nucleon [61].

In the most recent experiment of the FAZIA Collaboration, isospin transport ratios were determined for cross bombardments of ^{58}Ni and ^{64}Ni projectiles and targets at 32 and 52 MeV/nucleon incident energy [6]. Increasing isospin equilibration with decreasing impact parameter is reported but full equilibration is not observed, even for the most central collisions. A very similar conclusion was presented very recently for the $^{40,48}\text{Ca} + ^{40,48}\text{Ca}$ system at 35 MeV/nucleon by Fable *et al.* who also applied the isospin transport-ratio technique [62]. These results emphasize the transitional nature of the Fermi energy domain with the effect that small differences in the reaction systems and the experimental conditions may manifest themselves in measurable differences of the observed isospin transport [63].

Contact times, if assumed to correspond to the sum of the diameters of the collision partners divided by the velocity of the projectile, are of the order of 70 fm/c in the present reaction and, depending on the impact parameter and dynamical details, may fall between 50 and 100 fm/c. This interval represents the timescale on which the observed isospin equilibration apparently occurs. It is also consistent with the time characterizing the statistical nucleation process in the neck region which is described within the freeze-out volume conception. Similar times of about 100 fm/c were found by Tsang *et al.* [60] to be needed for the observed isospin diffusion in the $^{112,124}\text{Sn} + ^{112,124}\text{Sn}$ collisions at 50 MeV/nucleon according to Boltzmann-Uehling-Uhlenbeck (BUU) calculations performed for these reactions. For the similar Xe + Sn system at 32 MeV/nucleon, isospin equilibration times of less than 200 fm/c were deduced from calculations with the stochastic mean field (SMF) model [64].

Equilibration times of very similar magnitude were deduced from an experiment of different type by Jedelev *et al.* [65]. There, the authors followed the isospin equilibration in a rotating dinuclear system formed by the decay of deformed projectile fragments produced in $^{70}\text{Zn} + ^{70}\text{Zn}$ collisions at 35 MeV/nucleon. For selected systems, the obtained equilibration times were of the order of 0.3 zs, corresponding to ≈ 100 fm/c, whereas the process up to full isospin equilibration may be followed for somewhat longer times [66]. It thus seems that, according to the presented examples, N/Z equilibration proceeds fast enough to be observed in the $^{80}\text{Kr} + ^{48,40}\text{Ca}$ experiments at 35 MeV/nucleon. It should be interesting to study the full charge range of projectile fragments and connect it with the evolution of the isospin transport. The measurements of correlated fragments, both in the neck and projectile regions, are important in this case.

The neutron richness of neck emissions has been reported by many authors [36, 62, 67–70] and deduced from theoretical work [38]. Thériault *et al.* have studied the symmetric $^{64}\text{Zn} + ^{64}\text{Zn}$ reaction at 45 MeV/nucleon [67]. They found that the completely reconstructed midrapidity material is more neutron rich than the overall reaction

system whereas the reconstructed N/Z ratio for the projectile system remains below that value. This result was presented by the authors as the most complete evidence, at that time, of neutron enrichment of midrapidity nuclear matter at the expense of the remaining reaction system, a phenomenon related to the density dependence of the nuclear symmetry energy. The reconstruction of the compositions of the projectile and neck source presented here for the $^{80}\text{Kr} + ^{48,40}\text{Ca}$ reactions is in full agreement with these earlier findings.

IX. SUMMARY

The isospin transport in the $^{80}\text{Kr} + ^{48}\text{Ca}$ and $^{80}\text{Kr} + ^{40}\text{Ca}$ reactions at 35 MeV/nucleon was studied with calculations using the statistical multifragmentation model (SMM, Ref. [13]) in comparison with the data reported by the FAZIA Collaboration [4]. Regarding the experimental data, it was assumed that the events recorded with four FAZIA blocks are representative for the mid-peripheral collisions of the studied reactions. In the analysis, the ensembles of excited sources formulated and verified in previous studies of ALADIN and other experimental data were considered as applicable for the present reactions, an assumption supported by the obtained very satisfactory representation of the measured isotopic distributions. The odd-even staggered $\langle N \rangle/Z$ pattern of light fragments and its relation to the composition of the source was assumed to be universally valid.

With these assumptions, the intermediate reaction system at the time of the transition from its dynamical creation to the assumed statistical decay was reconstructed by identifying it with the ensemble of sources whose decay is treated with the SMM. It was found that the isospin exchange leads the intermediate system to cover at least half of the way to equilibrium. The most probable value of $87 \pm 11\%$, in fact, does not exclude full equilibrium. The reconstructed compositions were found to be slightly reduced in neutrons with respect to the equilibrium compositions by amounts corresponding to a loss of about two neutrons, similar for both reactions.

The compositions of the sources responsible for the production of the two groups of light fragments with $Z \leq 4$ were found to be significantly different. For the group with longitudinal velocities larger than those of the coincident heavier fragments, the source composition is similar to that of the heavier fragments, indicating that both, the heavier and the lighter fragments, originate from the breakup of the same intermediate system. The sources of light fragments with longitudinal velocities smaller than those of the coincident heavier fragments were found to be enriched in neutrons beyond the values expected for mixed systems consisting of equal numbers of nucleons from the projectile and from the target. The assumption of a low-density neck region, enriched in neutrons and with a mass of the order of 25 nucleons, provided a consistent explanation.

These conclusions are based on SMM calculations using ensembles of excited sources as initial configurations whose decay is assumed to be statistical and followed according to the model. The simultaneous consideration of two correlated statistical sources, one representing the projectile residues and one describing the excited low-density matter in the neck region, represents a novel theoretical development. The applicability of the method was demonstrated by satisfactorily reproducing the reported isotope distributions with reasonable assumptions regarding the effect of the target composition in forming the excited projectile residues.

In the second part of the analysis, the isotopic composition of the ensemble was systematically varied and the agreement of the calculated and experimental results quantitatively evaluated. Two methods were used, one of comparing the experimental and theoretical mean $\langle N \rangle / Z$ values, and the other of minimizing the χ^2 of the reproduction of the measured isotope distributions by using the experimental errors. Both methods were found to yield consistent results. The $\langle N \rangle / Z$ pattern as a function of Z of fragments from the neck-type source was success-

fully described by assuming a lower density and higher excitation energy. These parameters are similar to those found in the statistical analyses of central nucleus-nucleus collisions at similar energies. Altogether, the chosen statistical approach using two correlated sources, was found applicable for studying isospin transport phenomena in mid-peripheral collisions in the Fermi energy domain.

Acknowledgments

The authors are grateful to S. Piantelli and the FAZIA Collaboration for providing published data in numerical form and to the ALADIN Collaboration for giving access to the S254 experimental data. R.O. gratefully acknowledges the support by TUBITAK (Turkish Scientific and Technological Research Council) under Project No. BIDEB-1059B192001096 and the warm hospitality of GSI. N.B., A.S.B., and M.B. acknowledge support from the DAAD/TUBITAK exchange program.

-
- [1] *Dynamics and Thermodynamics with Nuclear Degrees of Freedom*, edited by Ph. Chomaz, F. Gulminelli, W. Trautmann, and S. J. Yennello (Springer, Berlin, 2006); Eur. Phys. J. A **30**, 1 (2006).
 - [2] *Topical Issue on Nuclear Symmetry Energy*, edited by Bao-An Li, A. Ramos, G. Verde, and I. Vidaña (Springer, Berlin, 2014); Eur. Phys. J. A **50**, 9 (2014).
 - [3] For examples see, e.g., B. Blank, T. Goigoux, P. Ascher, M. Gerbaux, J. Giovannazzo, S. Grévy *et al.*, Phys. Rev. C **93**, 061301 (2016); K. Schmidt, X. Cao, E. J. Kim, K. Hagel, M. Barbu, J. Gauthier *et al.*, *ibid.* **95**, 054618 (2017).
 - [4] S. Piantelli, G. Casini, A. Ono, G. Poggi, G. Pastore, S. Barlini *et al.*, Phys. Rev. C **103**, 014603 (2021).
 - [5] A. Camaiani, G. Casini, S. Piantelli, A. Ono, E. Bonnet, R. Alba *et al.*, Phys. Rev. C **103**, 014605 (2021).
 - [6] C. Ciampi, S. Piantelli, G. Casini, G. Pasquali, J. Quicray, L. Baldesi *et al.*, Phys. Rev. C **106**, 024603 (2022).
 - [7] R. Bougault, G. Poggi, S. Barlini, B. Borderie, G. Casini, A. Chbihi *et al.*, Eur. Phys. J. A **50**, 47 (2014).
 - [8] G. Pastore, D. Gruyer, P. Ottanelli, N. Le Neindre, G. Pasquali, R. Alba *et al.*, Nucl. Instrum. Methods Phys. Res. A **860**, 42 (2017).
 - [9] V. Baran, M. Colonna, V. Greco, and M. Di Toro, Phys. Rep. **410**, 335 (2005).
 - [10] Bao-An Li, Lie-Wen Chen, and Che Ming Ko, Phys. Rep. **464**, 113 (2008).
 - [11] N. T. Porile and L. B. Church, Phys. Rev. **133**, B310 (1964).
 - [12] T. H. Ku and P. J. Karol, Phys. Rev. C **16**, 1984 (1977).
 - [13] J. P. Bondorf, A. S. Botvina, A. S. Iljinov, I. N. Mishustin, and K. Sneppen, Phys. Rep. **257**, 133 (1995).
 - [14] A. S. Botvina, I. N. Mishustin, M. Begemann-Blaich, J. Hubele, G. Imme, I. Iori *et al.*, Nucl. Phys. A **584**, 737 (1995).
 - [15] Hongfei Xi, T. Odeh, R. Bassini, M. Begemann-Blaich, A. S. Botvina, S. Fritz *et al.*, Z. Phys. A **359**, 397 (1997); H. Xi *et al.*, Eur. Phys. J. A **1**, 235(E) (1998).
 - [16] R. Ogul, A. S. Botvina, U. Atav, N. Buyukcizmeci, I. N. Mishustin, P. Adrich *et al.*, Phys. Rev. C **83**, 024608 (2011); **85**, 019903(E) (2012).
 - [17] H. Imal, A. Ergun, N. Buyukcizmeci, R. Ogul, A. S. Botvina, and W. Trautmann, Phys. Rev. C **91**, 034605 (2015).
 - [18] M. D'Agostino, A. S. Botvina, P. M. Milazzo, M. Bruno, G. J. Kunde, D. R. Bowman *et al.*, Phys. Lett. B **371**, 175 (1996).
 - [19] N. Bellaize, O. Lopez, J. P. Wieleczko, D. Cussol, G. Auger, Ch. O. Bacri *et al.*, Nucl. Phys. A **709**, 367 (2002).
 - [20] J. Iglio, D. V. Shetty, S. J. Yennello, G. A. Souliotis, M. Jandel, A. L. Keksis, S. N. Soisson, B. C. Stein, S. Wuenschel, and A. S. Botvina, Phys. Rev. C **74**, 024605 (2006).
 - [21] A. S. Botvina and I. N. Mishustin, Eur. Phys. J. A **30**, 121 (2006).
 - [22] H. Imal, N. Buyukcizmeci, R. Ogul, and A. S. Botvina, Eur. Phys. J. A **56**, 110 (2020).
 - [23] M. Di Toro, A. Olmi, and R. Roy, Eur. Phys. J. A **30**, 65 (2006).
 - [24] N. Bohr, Nature **137**, 344 (1936).
 - [25] R. J. Charity, M. A. McMahan, G. J. Wozniak, R. J. McDonald, L. G. Moretto, D. G. Sarantites *et al.*, Nucl. Phys. A **483**, 371 (1988).
 - [26] R. J. Charity, K. X. Jing, D. R. Bowman, M. A. McMahan, G. J. Wozniak, L. G. Moretto *et al.*, Nucl. Phys. A **511**, 59 (1990).
 - [27] L. Pienkowski, K. Kwiatkowski, T. Lefort, W.-c. Hsi, L. Beaulieu, V. E. Viola *et al.*, Phys. Rev. C **65**, 064606 (2002).
 - [28] D. H. E. Gross, Rep. Prog. Phys. **53**, 605 (1990).

- [29] A. S. Botvina, N. Buyukcizmeci, and M. Bleicher, Phys. Rev. C **103**, 064602 (2021).
- [30] A. S. Botvina, N. Buyukcizmeci, and M. Bleicher, Phys. Rev. C **106**, 014607 (2022).
- [31] T. Furuta and A. Ono, Phys. Rev. C **79**, 014608 (2009).
- [32] A. H. Raduta, M. Colonna, and M. Di Toro, Phys. Rev. C **76**, 024602 (2007).
- [33] R. J. Charity, Phys. Rev. C **58**, 1073 (1998).
- [34] C. P. Montoya, W. G. Lynch, D. R. Bowman, G. F. Peaslee, N. Carlin, R. T. deSouza *et al.*, Phys. Rev. Lett. **73**, 3070 (1994).
- [35] J. F. Dempsey, R. J. Charity, L. G. Sobotka, G. J. Kunde, S. Gaff, C. K. Gelbke *et al.*, Phys. Rev. C **54**, 1710 (1996).
- [36] J. Lukasik, J. Benlliure, V. Métivier, E. Plagnol, B. Tamain, M. Assenard *et al.*, Phys. Rev. C **55**, 1906 (1997).
- [37] S. Piantelli, L. Bidini, G. Poggi, M. Bini, G. Casini, P. R. Maurenzig, A. Olmi, G. Pasquali, A. A. Stefanini, and N. Taccetti, Phys. Rev. Lett. **88**, 052701 (2002).
- [38] V. Baran, M. Colonna, and M. Di Toro, Nucl. Phys. A **730**, 329 (2004).
- [39] S. Hudan, R. Alfaro, L. Beaulieu, B. Davin, Y. Larochelle, T. Lefort *et al.*, Phys. Rev. C **70**, 031601(R) (2004).
- [40] A. Ergun, H. Imal, N. Buyukcizmeci, R. Ogul, and A. S. Botvina, Phys. Rev. C **92**, 014610 (2015).
- [41] A. S. Botvina and I. N. Mishustin, Phys. Rev. C **63**, 061601(R) (2001).
- [42] V. Baran, M. Colonna, M. Di Toro, M. Zielinska-Pfabe, and H. H. Wolter, Phys. Rev. C **72**, 064620 (2005).
- [43] S. Piantelli, G. Casini, A. Ono, G. Poggi, G. Pastore, S. Barlini *et al.*, Phys. Rev. C **101**, 034613 (2020).
- [44] S. Hudan, R. T. de Souza, and A. Ono, Phys. Rev. C **73**, 054602 (2006).
- [45] A. S. Botvina, K. K. Gudima, J. Steinheimer, M. Bleicher, and J. Pochodzalla, Phys. Rev. C **95**, 014902 (2017).
- [46] A. S. Botvina, A. S. Iljinov, and I. N. Mishustin, Yad. Fiz. **42**, 1127 (1985) [Sov. J. Nucl. Phys. **42**, 712 (1985)].
- [47] A. S. Botvina, O. V. Lozhkin, and W. Trautmann, Phys. Rev. C **65**, 044610 (2002).
- [48] N. Buyukcizmeci, R. Ogul, and A. S. Botvina, Eur. Phys. J. A **25**, 57 (2005).
- [49] G. A. Souliotis, A. S. Botvina, D. V. Shetty, A. L. Keksis, M. Jandel, M. Veselsky, and S. J. Yennello, Phys. Rev. C **75**, 011601(R) (2007).
- [50] S. Hudan, A. B. McIntosh, J. Black, D. Mercier, C. J. Metelko, R. Yanez *et al.*, Phys. Rev. C **80**, 064611 (2009).
- [51] A. Le Fèvre, G. Auger, M. L. Begemann-Blaich, N. Bellaize, R. Bittiger, F. Bocage *et al.*, Phys. Rev. Lett. **94**, 162701 (2005).
- [52] Ad. R. Raduta and F. Gulminelli, Phys. Rev. C **75**, 024605 (2007).
- [53] A. Ono, P. Danielewicz, W. A. Friedman, W. G. Lynch, and M. B. Tsang, Phys. Rev. C **70**, 041604(R) (2004).
- [54] S. Barlini, S. Piantelli, G. Casini, P. R. Maurenzig, A. Olmi, M. Bini *et al.*, Phys. Rev. C **87**, 054607 (2013).
- [55] W. Trautmann, Nucl. Phys. A **787**, 575c (2007).
- [56] J. Lukasik, P. Adrich, T. Aumann, C. O. Bacri, T. Barczyk, R. Bassini *et al.*, Nucl. Instrum. Methods Phys. Res. A **587**, 413 (2008).
- [57] D. Henzlova, K. H. Schmidt, M. V. Ricciardi, A. Kelić, V. Henzl, P. Napolitani *et al.*, Phys. Rev. C **78**, 044616 (2008).
- [58] J. Colin, D. Cussol, J. Normand, N. Bellaize, R. Bougault, A. M. Buta *et al.*, Phys. Rev. C **67**, 064603 (2003).
- [59] H. Johnston, T. White, J. Winger, D. Rowland, B. Hurst, F. Gimeno-Nogues, D. O’Kelly, and S. J. Yennello, Phys. Lett. B **371**, 186 (1996).
- [60] M. B. Tsang, T. X. Liu, L. Shi, P. Danielewicz, C. K. Gelbke, X. D. Liu *et al.*, Phys. Rev. Lett. **92**, 062701 (2004).
- [61] A. L. Keksis, L. W. May, G. A. Souliotis, M. Veselsky, S. Galanopoulos, Z. Kohley *et al.*, Phys. Rev. C **81**, 054602 (2010).
- [62] Q. Fable, A. Chbihi, J. D. Frankland, P. Napolitani, G. Verde, E. Bonnet *et al.*, Phys. Rev. C **107**, 014604 (2023).
- [63] D. D. S. Coupland, W. G. Lynch, M. B. Tsang, P. Danielewicz, and Y. Zhang, Phys. Rev. C **84**, 054603 (2011).
- [64] G. Ademard, B. Borderie, A. Chbihi, O. Lopez, P. Napolitani, M. F. Rivet *et al.*, Eur. Phys. J. A **50**, 33 (2014).
- [65] A. Jede, A. B. McIntosh, K. Hagel, M. Huang, L. Heilborn, Z. Kohley *et al.*, Phys. Rev. Lett. **118**, 062501 (2017).
- [66] K. Brown, S. Hudan, R. T. deSouza, J. Gauthier, R. Roy, D. V. Shetty, G. A. Souliotis, and S. J. Yennello, Phys. Rev. C **87**, 061601(R) (2013).
- [67] D. Thériault, J. Gauthier, F. Grenier, F. Moisan, C. St-Pierre, R. Roy *et al.*, Phys. Rev. C **74**, 051602(R) (2006).
- [68] Z. Kohley, L. W. May, S. Wuenschel, M. Colonna, M. Di Toro, M. Zielinska-Pfabe *et al.*, Phys. Rev. C **83**, 044601 (2011).
- [69] E. De Filippo, A. Pagano, P. Russotto, F. Amorini, A. Anzalone, L. Auditore *et al.*, Phys. Rev. C **86**, 014610 (2012).
- [70] R. Bougault, E. Bonnet, B. Borderie, A. Chbihi, D. Dell’Aquila, Q. Fable *et al.*, Phys. Rev. C **97**, 024612 (2018).